

ARTICLES

Ratios of bottom meson branching fractions involving J/ψ mesons and determination of b quark fragmentation fractions

- F. Abe,¹⁴ H. Akimoto,³² A. Akopian,²⁷ M. G. Albrow,⁷ S. R. Amendolia,²³ D. Amidei,¹⁷ J. Antos,²⁹ C. Anway-Wiese,⁴ S. Aota,³² G. Apollinari,²⁷ T. Asakawa,³² W. Ashmanskas,¹⁵ M. Atac,⁷ F. Azfar,²² P. Azzi-Bacchetta,²¹ N. Bacchetta,²¹ W. Badgett,¹⁷ S. Bagdasarov,²⁷ M. W. Bailey,¹⁹ J. Bao,³⁵ P. de Barbaro,²⁶ A. Barbaro-Galtieri,¹⁵ V. E. Barnes,²⁵ B. A. Barnett,¹³ E. Barzi,⁸ G. Bauer,¹⁶ T. Baumann,⁹ F. Bedeschi,²³ S. Behrends,³ S. Belforte,²³ G. Bellettini,²³ J. Bellinger,³⁴ D. Benjamin,³¹ J. Benlloch,¹⁶ J. Bensinger,³ D. Benton,²² A. Beretvas,⁷ J. P. Berge,⁷ J. Berryhill,⁵ S. Bertolucci,⁸ B. Bevensee,²² A. Bhatti,²⁷ K. Biery,¹² M. Binkley,⁷ D. Bisello,²¹ R. E. Blair,¹ C. Blocker,³ A. Bodek,²⁶ W. Bokhari,¹⁶ G. Bolla,²¹ V. Bolognesi,⁷ D. Bortoletto,²⁵ J. Boudreau,²⁴ L. Breccia,² C. Bromberg,¹⁸ N. Bruner,¹⁹ E. Buckley-Geer,⁷ H. S. Budd,²⁶ K. Burkett,¹⁷ G. Busetto,²¹ A. Byon-Wagner,⁷ K. L. Byrum,¹ J. Cammerata,¹³ C. Campagnari,⁷ M. Campbell,¹⁷ A. Caner,⁷ W. Carithers,¹⁵ D. Carlsmith,³⁴ A. Castro,²¹ D. Cauz,²³ Y. Cen,²⁶ F. Cervelli,²³ P. S. Chang,²⁹ P. T. Chang,²⁹ H. Y. Chao,²⁹ J. Chapman,¹⁷ M.-T. Cheng,²⁹ G. Chiarelli,²³ T. Chikamatsu,³² C. N. Chiou,²⁹ L. Christofek,¹¹ S. Cihangir,⁷ A. G. Clark,²³ M. Cobal,²³ M. Contreras,⁵ J. Conway,²⁸ J. Cooper,⁷ M. Cordelli,⁸ C. Couyoumtzelis,²³ D. Crane,¹ D. Cronin-Hennessy,⁶ R. Culbertson,⁵ J. D. Cunningham,³ T. Daniels,¹⁶ F. DeJongh,⁷ S. Delchamps,⁷ S. Dell'Agnello,²³ M. Dell'Orso,²³ R. Demina,⁷ L. Demortier,²⁷ B. Denby,²³ M. Deninno,² P. F. Derwent,¹⁷ T. Devlin,²⁸ J. R. Dittmann,⁶ S. Donati,²³ J. Done,³⁰ T. Dorigo,²¹ A. Dunn,¹⁷ N. Eddy,¹⁷ K. Einsweiler,¹⁵ J. E. Elias,⁷ R. Ely,¹⁵ E. Engels, Jr.,²⁴ D. Errede,¹¹ S. Errede,¹¹ Q. Fan,²⁶ I. Fiori,² B. Flaughner,⁷ G. W. Foster,⁷ M. Franklin,⁹ M. Frautschi,³¹ J. Freeman,⁷ J. Friedman,¹⁶ T. A. Fuess,¹ Y. Fukui,¹⁴ S. Funaki,³² G. Gagliardi,²³ S. Galeotti,²³ M. Gallinaro,²¹ M. Garcia-Sciveres,¹⁵ A. F. Garfinkel,²⁵ C. Gay,⁹ S. Geer,⁷ D. W. Gerdes,¹³ P. Giannetti,²³ N. Giokaris,²⁷ P. Giromini,⁸ L. Gladney,²² D. Glenzinski,¹³ M. Gold,¹⁹ J. Gonzalez,²² A. Gordon,⁹ A. T. Goshaw,⁶ K. Goulianos,²⁷ H. Grassmann,²³ L. Groer,²⁸ C. Grosso-Pilcher,⁵ G. Guillian,¹⁷ R. S. Guo,²⁹ C. Haber,¹⁵ E. Hafen,¹⁶ S. R. Hahn,⁷ R. Hamilton,⁹ R. Handler,³⁴ R. M. Hans,³⁵ K. Hara,³² A. D. Hardman,²⁵ B. Harral,²² R. M. Harris,⁷ S. A. Hauger,⁶ J. Hauser,⁴ C. Hawk,²⁸ E. Hayashi,³² J. Heinrich,²² K. D. Hoffman,²⁵ M. Hohlmann,¹⁵ C. Holck,²² R. Hollebeek,²² L. Holloway,¹¹ A. Holscher,¹² S. Hong,¹⁷ G. Houk,²² P. Hu,²⁴ B. T. Huffman,²⁴ R. Hughes,²⁶ J. Huston,¹⁸ J. Huth,⁹ J. Hylen,⁷ H. Ikeda,³² M. Incagli,²³ J. Incandela,⁷ G. Introzzi,²³ J. Iwai,³² Y. Iwata,¹⁰ H. Jensen,⁷ U. Joshi,⁷ R. W. Kadel,¹⁵ E. Kajfasz,^{7,*} H. Kambara,²³ T. Kamon,³⁰ T. Kaneko,³² K. Karr,³³ H. Kasha,³⁵ Y. Kato,²⁰ T. A. Keaffaber,²⁵ L. Keeble,⁸ K. Kelley,¹⁶ R. D. Kennedy,²⁸ R. Kephart,⁷ P. Kesten,¹⁵ D. Kestenbaum,⁹ R. M. Keup,¹¹ H. Keutelian,⁷ F. Keyvan,⁴ B. Kharadia,¹¹ B. J. Kim,²⁶ D. H. Kim,^{7,*} H. S. Kim,¹² S. B. Kim,¹⁷ S. H. Kim,³² Y. K. Kim,¹⁵ L. Kirsch,³ P. Koehn,²⁶ K. Kondo,³² J. Konigsberg,⁹ S. Kopp,⁵ K. Kordas,¹² A. Korytov,¹⁶ W. Koska,⁷ E. Kovacs,^{7,*} W. Kowald,⁶ M. Krasberg,¹⁷ J. Kroll,⁷ M. Kruse,²⁵ T. Kuwabara,³² S. E. Kuhlmann,¹ E. Kuns,²⁸ A. T. Laasanen,²⁵ N. Labanca,²³ S. Lammel,⁷ J. I. Lamoureux,³ T. LeCompte,¹ S. Leone,²³ J. D. Lewis,⁷ P. Limon,⁷ M. Lindgren,⁴ T. M. Liss,¹¹ N. Lockyer,²² O. Long,²² C. Loomis,²⁸ M. Loretì,²¹ J. Lu,³⁰ D. Lucchesi,²³ P. Lukens,⁷ S. Lusin,³⁴ J. Lys,¹⁵ K. Maeshima,⁷ A. Maghakian,²⁷ P. Maksimovic,¹⁶ M. Mangano,²³ J. Mansour,¹⁸ M. Mariotti,²¹ J. P. Marriner,⁷ A. Martin,¹¹ J. A. J. Matthews,¹⁹ R. Mattingly,¹⁶ P. McIntyre,³⁰ P. Melese,²⁷ A. Menzione,²³ E. Meschi,²³ S. Metzler,²² C. Miao,¹⁷ T. Miao,⁷ G. Michail,⁹ R. Miller,¹⁸ H. Minato,³² S. Miscetti,⁸ M. Mishina,¹⁴ H. Mitsushio,³² T. Miyamoto,³² S. Miyashita,³² N. Moggi,²³ Y. Morita,¹⁴ J. Mueller,²⁴ A. Mukherjee,⁷ T. Muller,⁴ P. Murat,²³ H. Nakada,³² I. Nakano,³² C. Nelson,⁷ D. Neuberger,⁴ C. Newman-Holmes,⁷ M. Ninomiya,³² L. Nodulman,¹ S. H. Oh,⁶ K. E. Ohl,³⁵ T. Ohmoto,¹⁰ T. Ohsugi,¹⁰ R. Oishi,³² M. Okabe,³² T. Okusawa,²⁰ R. Oliveira,²² J. Olsen,³⁴ C. Pagliarone,² R. Paoletti,²³ V. Papadimitriou,³¹ S. P. Pappas,³⁵ S. Park,⁷ A. Parri,⁸ J. Patrick,⁷ G. Pauletta,²³ M. Paulini,¹⁵ A. Perazzo,²³ L. Pescara,²¹ M. D. Peters,¹⁵ T. J. Phillips,⁶ G. Piacentino,² M. Pillai,²⁶ K. T. Pitts,⁷ R. Plunkett,⁷ L. Pondrom,³⁴ J. Proudfoot,¹ F. Ptohos,⁹ G. Punzi,²³ K. Ragan,¹² A. Ribon,²¹ F. Rimondi,² L. Ristori,²³ W. J. Robertson,⁶ T. Rodrigo,^{7,*} S. Rolli,²³ J. Romano,⁵ L. Rosenson,¹⁶ R. Roser,¹¹ W. K. Sakumoto,²⁶ D. Saltzberg,⁵ A. Sansoni,⁸ L. Santi,²³ H. Sato,³² V. Scarpine,³⁰ P. Schlabach,⁹ E. E. Schmidt,⁷ M. P. Schmidt,³⁵ A. Scribano,²³ S. Segler,⁷ S. Seidel,¹⁹ Y. Seiya,³² G. Sganos,¹² M. D. Shapiro,¹⁵ N. M. Shaw,²⁵ Q. Shen,²⁵ P. F. Shepard,²⁴ M. Shimojima,³² M. Shochet,⁵ J. Siegrist,¹⁵ A. Sill,³¹ P. Sinervo,¹² P. Singh,²⁴ J. Skarha,¹³ K. Sliwa,³³ F. D. Snider,¹³ T. Song,¹⁷ J. Spalding,⁷ T. Speer,²³ P. Sphicas,¹⁶ F. Spinella,²³ M. Spiropulu,⁹ L. Spiegel,⁷ L. Stanco,²¹ J. Steele,³⁴ A. Stefanini,²³ K. Strahl,¹² J. Strait,⁷ R. Ströhmer,⁹ D. Stuart,⁷ G. Sullivan,⁵ A. Soumarokov,²⁹ K. Sumorok,¹⁶ J. Suzuki,³² T. Takada,³² T. Takahashi,²⁰ T. Takano,³² K. Takikawa,³² N. Tamura,¹⁰ F. Tartarelli,²³ W. Taylor,¹² P. K. Teng,²⁹ Y. Teramoto,²⁰ S. Tether,¹⁶ D. Theriot,⁷ T. L. Thomas,¹⁹ R. Thun,¹⁷ M. Timko,³³ P. Tipton,²⁶ A. Titov,²⁷ S. Tkaczyk,⁷ D. Toback,⁵ K. Tollefson,²⁶ A. Tollestrup,⁷ J. Tonnison,²⁵ J. F. de Troconiz,⁹ S. Truitt,¹⁷ J. Tseng,¹³ N. Turini,²³ T. Uchida,³² N. Uemura,³² F. Ukegawa,²² G. Unal,²² J. Valls,⁷ S. C. van den Brink,²⁴ S. Vejcik, III,¹⁷ G. Velez,²³ R. Vidal,⁷ M. Vondracek,¹¹ D. Vucinic,¹⁶ R. G. Wagner,¹ R. L. Wagner,⁷ J. Wahl,⁵ C. Wang,⁶ C. H. Wang,²⁹ G. Wang,²³ J. Wang,⁵ M. J. Wang,²⁹ Q. F. Wang,²⁷ A. Warburton,¹² T. Watts,²⁸ R. Webb,³⁰ C. Wei,⁶ C. Wendt,³⁴ H. Wenzel,¹⁵ W. C. Wester, III,⁷ A. B. Wicklund,¹ E. Wicklund,⁷ R. Wilkinson,²² H. H. Williams,²² P. Wilson,⁵ B. L. Winer,²⁶ D. Wolinski,¹⁷ J. Wolinski,¹⁸ X. Wu,²³ J. Wyss,²¹ A. Yagil,⁷ W. Yao,¹⁵

K. Yasuoka,³² Y. Ye,¹² G. P. Yeh,⁷ P. Yeh,²⁹ M. Yin,⁶ J. Yoh,⁷ C. Yosef,¹⁸ T. Yoshida,²⁰ D. Yovanovitch,⁷ I. Yu,³⁵
 L. Yu,¹⁹ J. C. Yun,⁷ A. Zanetti,²³ F. Zetti,²³ L. Zhang,³⁴ W. Zhang,²² and S. Zucchelli,²
 (CDF Collaboration)

¹Argonne National Laboratory, Argonne, Illinois 60439

²Istituto Nazionale di Fisica Nucleare, University of Bologna, I-40126 Bologna, Italy

³Brandeis University, Waltham, Massachusetts 02254

⁴University of California at Los Angeles, Los Angeles, California 90024

⁵University of Chicago, Chicago, Illinois 60637

⁶Duke University, Durham, North Carolina 27708

⁷Fermi National Accelerator Laboratory, Batavia, Illinois 60510

⁸Laboratori Nazionali di Frascati, Istituto Nazionale di Fisica Nucleare, I-00044 Frascati, Italy

⁹Harvard University, Cambridge, Massachusetts 02138

¹⁰Hiroshima University, Higashi-Hiroshima 724, Japan

¹¹University of Illinois, Urbana, Illinois 61801

¹²Institute of Particle Physics, McGill University, Montreal, Canada H3A 2T8

and University of Toronto, Toronto, Canada M5S 1A7

¹³The Johns Hopkins University, Baltimore, Maryland 21218

¹⁴National Laboratory for High Energy Physics (KEK), Tsukuba, Ibaraki 305, Japan

¹⁵Ernest Orland Lawrence Berkeley Laboratory, Berkeley, California 94720

¹⁶Massachusetts Institute of Technology, Cambridge, Massachusetts 02139

¹⁷University of Michigan, Ann Arbor, Michigan 48109

¹⁸Michigan State University, East Lansing, Michigan 48824

¹⁹University of New Mexico, Albuquerque, New Mexico 87131

²⁰Osaka City University, Osaka 588, Japan

²¹Universita di Padova, Istituto Nazionale di Fisica Nucleare, Sezione di Padova, I-35131 Padova, Italy

²²University of Pennsylvania, Philadelphia, Pennsylvania 19104

²³Istituto Nazionale di Fisica Nucleare, University and Scuola Normale Superiore of Pisa, I-56100 Pisa, Italy

²⁴University of Pittsburgh, Pittsburgh, Pennsylvania 15260

²⁵Purdue University, West Lafayette, Indiana 47907

²⁶University of Rochester, Rochester, New York 14627

²⁷Rockefeller University, New York, New York 10021

²⁸Rutgers University, Piscataway, New Jersey 08854

²⁹Academia Sinica, Taipei, Taiwan 11529, Republic of China

³⁰Texas A&M University, College Station, Texas 77843

³¹Texas Tech University, Lubbock, Texas 79409

³²University of Tsukuba, Tsukuba, Ibaraki 305, Japan

³³Tufts University, Medford, Massachusetts 02155

³⁴University of Wisconsin, Madison, Wisconsin 53706

³⁵Yale University, New Haven, Connecticut 06511

(Received 4 June 1996)

We report a measurement of the ratios of the decay rates of the B^+ , B^0 , and B_s^0 mesons into exclusive final states containing a J/ψ meson. The final states were selected from 19.6 pb^{-1} of $p\bar{p}$ collisions recorded by the Collider Detector at Fermilab. These data are interpreted to determine the b quark fragmentation fractions f_u , f_d , and f_s . We also determine the branching fractions for the decay modes $B^+ \rightarrow J/\psi K^+$, $B^+ \rightarrow J/\psi K^*(892)^+$, $B^0 \rightarrow J/\psi K^0$, $B^0 \rightarrow J/\psi K^*(892)^0$, and $B_s^0 \rightarrow J/\psi \phi(1020)$. We discuss the implications of these measurements to B meson decay models. [S0556-2821(96)04023-4]

PACS number(s): 13.25.Hw, 13.87.Fh, 14.40.Nd

I. INTRODUCTION

The bound states of bottom quarks provide a laboratory in which we can investigate the behavior of the strong force (quantum chromodynamics or QCD) and the electroweak interaction [1]. The lowest-lying bound states are the pseudo-scalar mesons (B^+ , B^0 , and B_s^0) formed by one bottom anti-quark bound to one of the three lightest quarks (u , d , and s ,

respectively). The branching fractions (\mathcal{B}) of these mesons into final states consisting of only hadrons (the fully hadronic decays) have been studied theoretically and have been shown to yield insights into the interactions that take place between a quark and antiquark pair at short distance scales [2–4].

Experimental studies of bottom meson hadronic decays have been limited by their relatively small branching fractions (typically 10^{-2} – 10^{-3}) and the difficulty of detecting the final states. The most precise branching fraction measurements have been made at e^+e^- colliders, where the B^+ and B^0 mesons are pair produced at threshold [5,6]. Bottom had-

*Visitor.

rons are produced copiously in high-energy proton-antiproton collisions [7–9] and so it is possible to measure the branching fractions of bottom mesons into those fully hadronic final states that have distinctive final state topologies. We report a study of the branching fractions of bottom mesons into final states consisting of a J/ψ meson and a light quark meson, using the Collider Detector at Fermilab (CDF). The data set consists of 19.6 pb^{-1} of 1.8 TeV $p\bar{p}$ collisions produced by the Fermilab Tevatron Collider. This work extends an earlier analysis of the same dataset [10] by incorporating an additional final state, $J/\psi\phi(1020)$, estimating the fragmentation fractions of B hadrons, and providing improved measurements of the branching fractions of B^+ and B^0 mesons. Throughout this paper, references to a specific decay mode imply the charge conjugate mode as well.

We have focused our study on the bottom meson decay modes that yield a J/ψ meson that subsequently decays to a $\mu^+\mu^-$ final state. This results in a signature that we can identify readily by using the CDF trigger system and provides the necessary rejection of other background processes. We have measured the observed cross-sections times branching fractions for the channels

$$B^+ \rightarrow J/\psi K^+, \quad (1)$$

$$B^0 \rightarrow J/\psi K^0, \quad (2)$$

$$B^+ \rightarrow J/\psi K^*(892)^+, \quad (3)$$

$$B^0 \rightarrow J/\psi K^*(892)^0, \quad (4)$$

$$B_s^0 \rightarrow J/\psi\phi(1020). \quad (5)$$

The observed cross section for the decay mode $B^+ \rightarrow J/\psi K^+$ can be decomposed into the form

$$\sigma_{\text{obs}} = \sigma(p\bar{p} \rightarrow \bar{b}) f_u \mathcal{B}(B^+ \rightarrow J/\psi K^+) \epsilon^{K^+}, \quad (6)$$

and similar forms can be written for the other decays. Here, $\sigma(p\bar{p} \rightarrow \bar{b})$ is the bottom antiquark production cross section and f_u is the probability that the fragmentation of a b antiquark will result in a B^+ meson. In a similar way, we define f_d and f_s to be the probabilities of a b antiquark to hadronize and form a B^0 and B_s^0 meson, respectively. We will refer to these probabilities as fragmentation fractions and include explicitly in this fraction contributions from decays of heavier B hadrons into final states containing a B^+ , B^0 , or B_s^0 meson. The expression $\mathcal{B}(B^+ \rightarrow J/\psi K^+)$ represents the branching fraction for this decay mode of the B^+ meson and ϵ^{K^+} is the efficiency of detecting the $J/\psi K^+$ final state.

The fragmentation fractions into the different B meson states are not well known. If one assumes that these fractions are independent of the flavor and energy of the quark initiating the hadronization process, then measurements of strange meson production in light quark fragmentation provide the most accurate estimates of f_s [11]. Only one measurement of f_s in the bottom meson system exists [12] and it has large uncertainties. No measurements have been made of f_u or f_d in the bottom meson system, despite the importance of these in many B hadron branching fraction, lifetime, and mixing studies [13,30].

The bottom quark production cross section $\sigma(p\bar{p} \rightarrow \bar{b})$ is not known precisely; the best measurements to date have uncertainties of order $\pm 20\%$ [9]. The efficiency ϵ^{K^+} depends on an understanding of the b quark production properties and detector acceptance. We, therefore, present our measurements in the form of ratios of branching fractions in order to avoid introducing additional uncertainties due to the b quark production cross section and the final state detection efficiency. We then compare these ratios directly with phenomenological predictions of the relative B meson branching fractions. We also use our data to estimate the fragmentation fractions f_u , f_d , and f_s .

We have organized this report as follows. In Sec. II, we describe the data selection and procedures that we followed to reconstruct the five decay modes. We present in Sec. III a study of the relative sizes of resonant and nonresonant $K\pi$ and KK contributions to the B meson final states. We describe the procedure used to determine the acceptance and efficiency corrections for each decay mode in Sec. IV. In Sec. V, we present the results of this study and conclude in Sec. VI.

II. DATA COLLECTION AND SELECTION

A. The CDF detector

CDF is a multipurpose detector designed to study high-energy $p\bar{p}$ collisions produced by the Fermilab Tevatron Collider. It surrounds the interaction point with three charged particle tracking detectors immersed in a 1.4 T solenoidal magnetic field. The tracking system is contained within a hermetic calorimeter system that measures the energy flow of charged and neutral particles. Charged particle detectors outside the calorimeter are used to identify muon candidates. The detector has a coordinate system with the z axis along the proton beam direction. The polar angle θ is defined relative to the z axis, r is the radius from this axis, and ϕ is the azimuthal angle. Pseudorapidity is defined as $\eta \equiv -\ln \tan(\theta/2)$.

The innermost tracking device is a silicon microstrip detector (SVX) located in the region between 3.0 and 7.9 cm in radius from the beam axis. This is followed by a set of time projection chambers (VTX) that measure charged particle trajectories out to a radius of 22 cm. An 84-layer drift chamber (CTC) measures the particle trajectories in the region between 30 and 130 cm in radius from the beam. This tracking system has high efficiency for detecting charged particles with momentum transverse to the beam $P_T > 0.35 \text{ GeV}/c$ and $|\eta| \leq 1.1$, and the CTC and SVX together measure charged particle transverse momenta with a precision of $\sigma_{P_T} \sim [(0.0066P_T)^2 + (0.0009P_T^2)^2]^{1/2}$ (with P_T in units of GeV/c).

The muon detection system consists of 4 layers of planar drift chambers separated from the interaction point by ~ 5 interaction lengths of material. Additional 4 layers of chambers are located outside the magnet return yoke (corresponding to 4 interaction lengths of material) in the central pseudorapidity region $|\eta| < 0.7$ to reduce the probability of misidentifying penetrating hadrons as muon candidates. An additional set of chambers is located in the pseudorapidity interval $0.7 < |\eta| < 1.0$ to extend the acceptance of the muon

system. The muon system is capable of detecting muons with $P_T \geq 1.4$ GeV/c in a pseudorapidity interval $|\eta| < 1.0$. These and other elements of the CDF detector are described in more detail elsewhere [14].

B. The J/ψ selection

We selected the J/ψ final state using a three-level trigger system that identified collisions with two muon candidates. The first level trigger required that there be two track candidates observed in the muon system. The level one trigger track efficiency rises from $\sim 40\%$ at $P_T = 1.5$ GeV/c to $\sim 93\%$ for muons with $P_T > 3$ GeV/c. The second level trigger requires the detection of a charged track in the CTC using the Central Fast Track processor (CFT), which performs a partial reconstruction of all charged tracks above a transverse momentum of ~ 2.5 GeV/c. The CTC track is required to match within 15° in ϕ of the muon candidate. The CFT efficiency rises from 40% at a muon $P_T = 2.6$ GeV/c to $\sim 94\%$ for $P_T > 3.1$ GeV/c. The third level trigger requires that two reconstructed CTC tracks match with two tracks in the muon chambers and that the dimuon invariant mass be between 2.8 and 3.4 GeV/c². The efficiency of the level three trigger requirement is $(97 \pm 2)\%$ for J/ψ candidates. There are 2.06×10^5 dimuon candidate events that passed the level three trigger requirements.

These events were further selected to identify a clean sample of J/ψ candidates. We required that each muon candidate have a CTC track candidate with $P_T > 1.4$ GeV/c. This track, when extrapolated to the muon chambers, was required to match within 3 standard deviations of the extrapolation and measurement uncertainties with a muon track in the transverse plane (r - ϕ) and along the beam axis direction. The two muon candidates were required to have opposite charges. We performed a least-squares fit of the two muon candidate tracks under the constraint that the two tracks come from a common point (a vertex constraint). We required the probability of this fit to be greater than 0.01. These requirements resulted in a signal of $(7.89 \pm 0.08) \times 10^4$ J/ψ decays on a background of nonresonant dimuon candidate events. The dimuon invariant mass distribution for this sample is shown in Fig. 1, along with an estimate of the background determined using same-charge muon candidate pairs. We performed an additional fit to the dimuon system, applying a vertex constraint and requiring that the dimuon invariant mass equal the world average J/ψ mass of 3.09688 GeV/c² [13]. The confidence level of this vertex-plus-mass constrained fit was required to be greater than 0.01.

C. Reconstruction of exclusive decays

1. The $B^+ \rightarrow J/\psi K^+$ channel

We reconstructed the exclusive decay modes listed in Eqs. (1)–(5) by forming charged particle combinations with the J/ψ candidate. For the decay channel $B^+ \rightarrow J/\psi K^+$, we considered every charged particle with $P_T > 1.5$ GeV/c as a K^+ candidate and required the resulting B^+ candidate to have $P_T > 8.0$ GeV/c. A least-squares fit was performed on the three charged tracks forming the $J/\psi K^+$ candidate by constraining the three tracks to come from a common vertex, the invariant mass of the dimuon system to equal the world

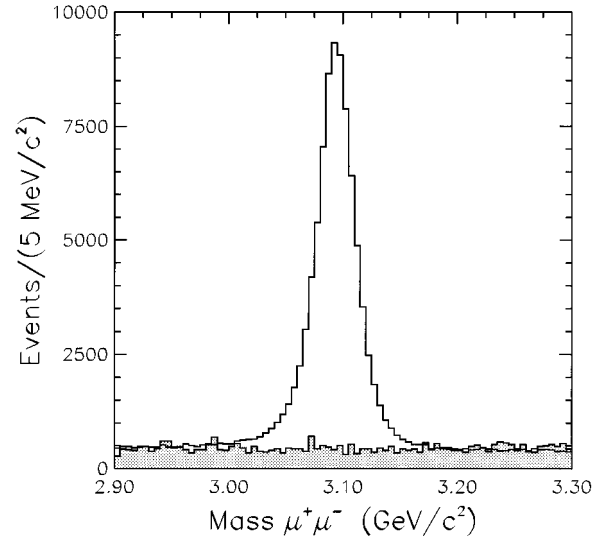


FIG. 1. The dimuon invariant mass distribution for the inclusive J/ψ event sample. The shaded distribution is for same-sign dimuon candidates.

average J/ψ mass, and the flight path of the B^+ candidate to be parallel to its momentum vector in the transverse plane (a two-dimensional pointing constraint). The confidence level of this least-squares fit had to exceed 0.01. We required the fitted transverse momenta of the muon candidate with lowest and highest P_T to be greater than 1.8 and 2.5 GeV/c, respectively. This ensured that the muon candidates were likely to pass the dimuon trigger requirements. In order to reduce the backgrounds from prompt J/ψ production, we required the B^+ meson candidate flight path to be pointing in the same hemisphere as its momentum vector (in effect requiring the B^+ candidate's observed proper decay length, $c\tau$, to be positive). The interaction vertex position was determined by averaging the measured beam position over a large number of collisions recorded under identical Tevatron Collider operating conditions. The $J/\psi K^+$ invariant mass distribution is shown in Fig. 2(a). We have performed a binned maximum likelihood fit of this data to a Gaussian line shape and a linear background term and estimate a B^+ signal of 154 ± 19 events. The width of the signal was not constrained in the fit and resulted in a fitted mass resolution of 0.015 ± 0.002 GeV/c², consistent with our expected detector resolution.

The reconstruction of the other four decay modes was performed with similar criteria in order to reduce the systematic uncertainties resulting from the kinematics of the produced B mesons and selection biases. Identical requirements were made on the quality and transverse momenta of the muon candidates, constraints on the fits to the B decay topologies, B meson lifetimes, and K_S^0 lifetimes. We allowed for small variations in the B and light quark meson transverse momentum requirements to optimize the expected significance for each channel. The significance is defined as $N_s / \sqrt{N_s + N_b}$, where N_s is the expected number of events determined using a Monte Carlo calculation for a given integrated luminosity, and N_b is the extrapolated background rate under the signal region using the observed B meson sideband background levels. This resulted in only modest differences in the P_T requirements from channel to channel,

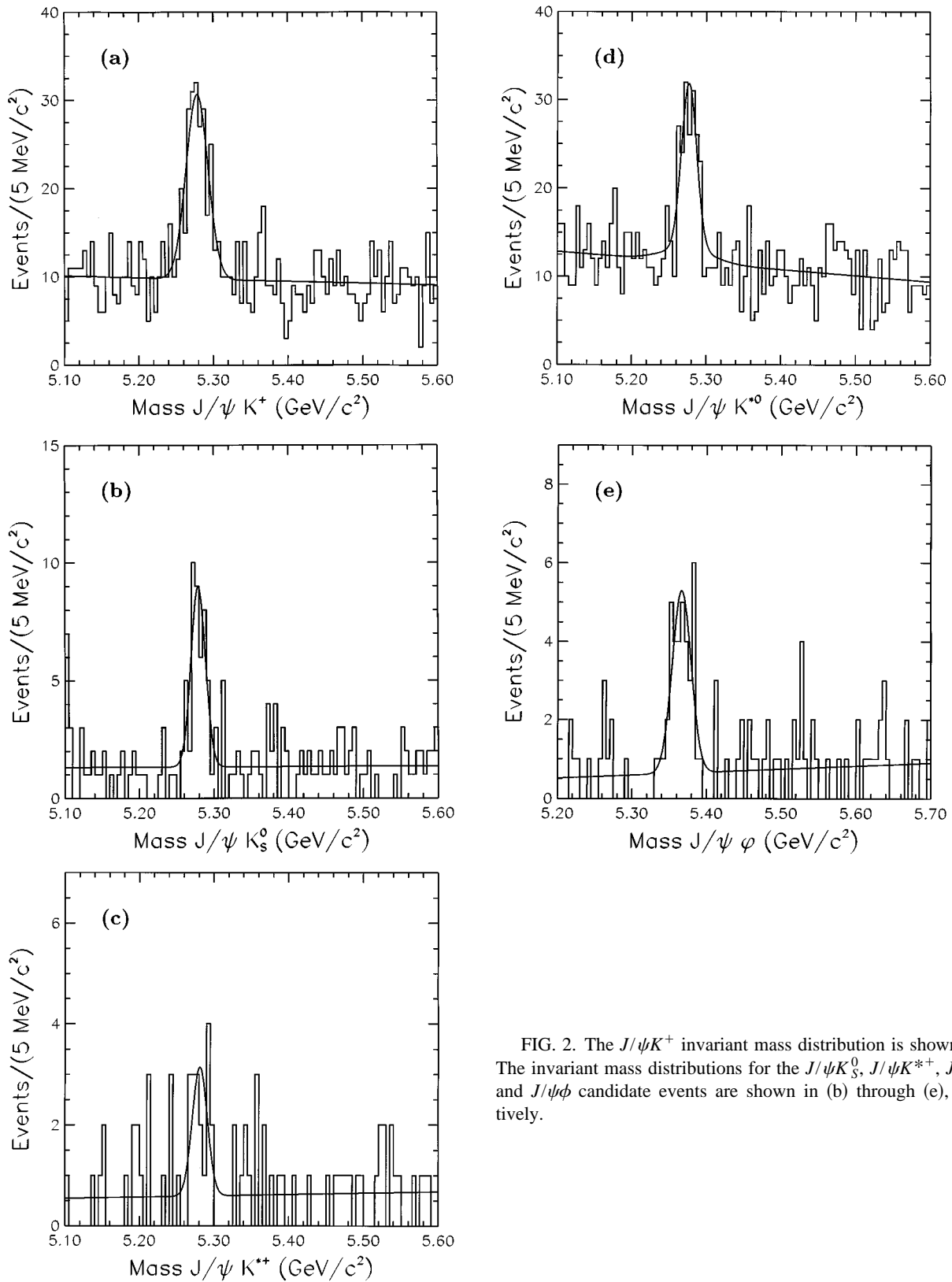


FIG. 2. The $J/\psi K^+$ invariant mass distribution is shown in (a). The invariant mass distributions for the $J/\psi K_S^0$, $J/\psi K^{*+}$, $J/\psi K^{*0}$, and $J/\psi \phi$ candidate events are shown in (b) through (e), respectively.

and did not introduce significant systematic uncertainties in our estimation of the B meson detection efficiency.

2. The $B^0 \rightarrow J/\psi K^0$ channel

The decay mode $B^0 \rightarrow J/\psi K^0$ was reconstructed by searching for $K^0 \rightarrow K_S^0 \rightarrow \pi^+ \pi^-$ candidates using all pairs of

oppositely charged particles. The daughter pions were required to have $P_T > 0.4$ GeV/c. To fully reconstruct the $B^0 \rightarrow J/\psi K_S^0$ decay, we performed a least-squares fit to the two pion candidate tracks and two muon candidates, constraining each track pair to come from common points, requiring the momentum vector of the K_S^0 candidate to point

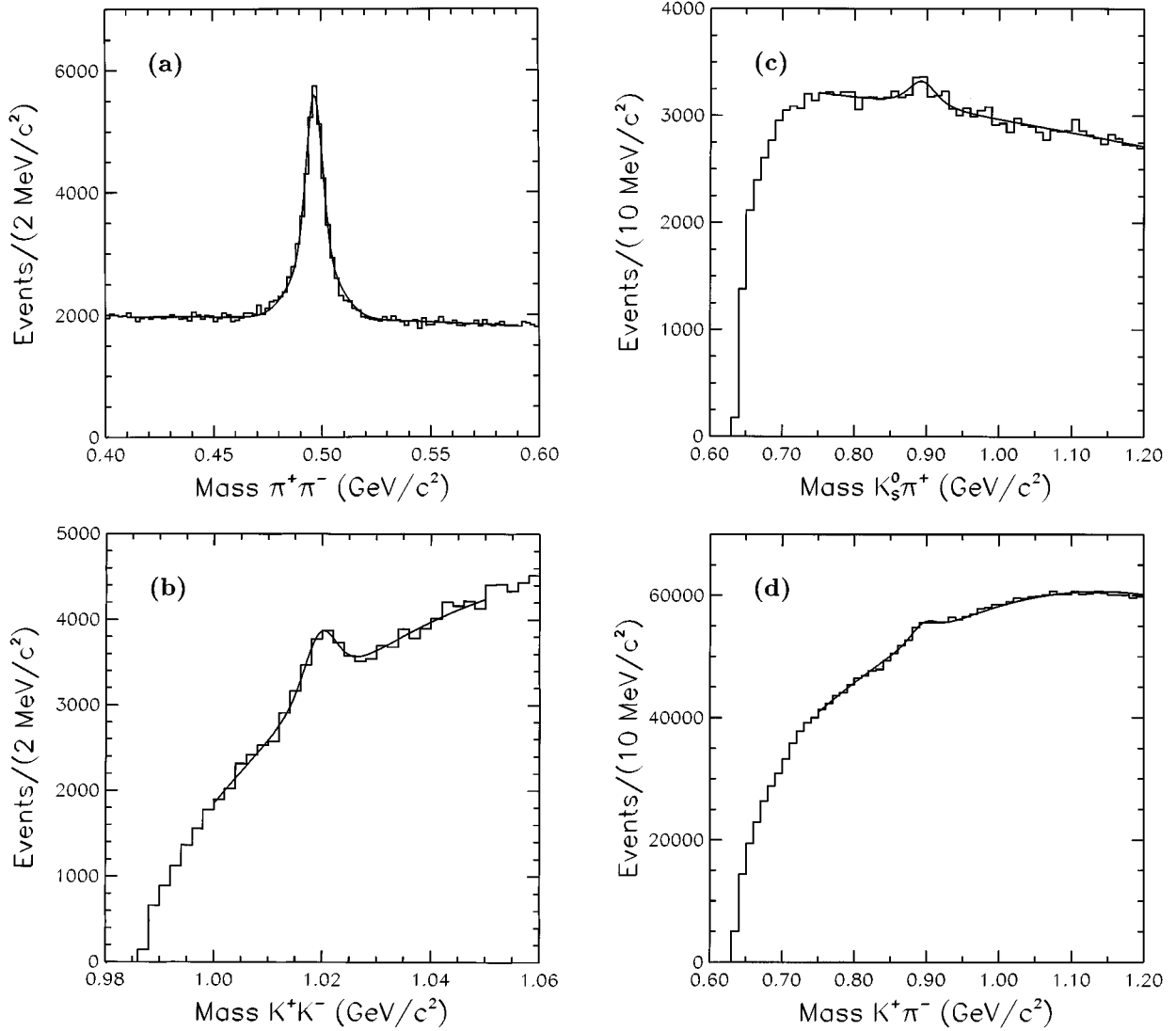


FIG. 3. The $\pi^+\pi^-$ invariant mass distribution is shown in (a) for K_S^0 candidates. The K^+K^- invariant mass distribution is shown in (b). The $K_S^0\pi^+$ invariant mass distribution is shown in (c). The $K^+\pi^-$ invariant mass distribution is shown in (d).

along its flight path (a vertex and pointing constraint) and placing a J/ψ mass constraint on the dimuon system. We also imposed a mass constraint on the dipion system, constraining the invariant $\pi^+\pi^-$ mass to the world average K_S^0 mass of $0.4977 \text{ GeV}/c^2$. The confidence level of the fit had to exceed 0.01. To improve the signal-to-noise ratio, we required the proper decay length of the K_S^0 candidate to be larger than 0.1 cm and its transverse momentum to be greater than 1.5 GeV/c . The $\pi^+\pi^-$ invariant mass distribution for the K_S^0 candidates that satisfy these requirements is illustrated in Fig. 3(a), and shows a K_S^0 signal of $(2.56 \pm 0.05) \times 10^4$ decays above a large combinatorial background (for illustration, no mass constraints were imposed in the least-squares fit to the charged tracks in this figure). To identify a clean B^0 candidate sample, we required the $J/\psi K_S^0$ candidates to have $P_T > 6.0 \text{ GeV}/c$ and the candidates to have a $c\tau$ greater than zero to reduce the combinatorial backgrounds from prompt J/ψ production. The invariant $J/\psi K_S^0$ mass distribution for these candidates is shown in Fig. 2(b). A fit of this distribution to a Gaussian line shape and linear background results in a total signal of $36.9 \pm 7.3 B^0$ decays.

3. The $B^+ \rightarrow J/\psi K^*(892)^+$ channel

We searched for the decay mode $B^+ \rightarrow J/\psi K^*(892)^+ \rightarrow J/\psi K_S^0 \pi^+$ by selecting a sample of J/ψ candidate events containing a K_S^0 candidate. The criteria used to identify K_S^0 candidates for the $J/\psi K_S^0$ final state also were used for this decay mode. We required the K_S^0 candidates to have $P_T > 2.0 \text{ GeV}/c$. We considered all other charged tracks with $P_T > 0.4 \text{ GeV}/c$ as π^+ candidates and we combined these with the K_S^0 candidates to form all possible $K^*(892)^+ \rightarrow K_S^0 \pi^+$ candidates. The combinatorial backgrounds to the $K^*(892)^+$ decay are large, as illustrated in the $K_S^0 \pi^+$ invariant mass distribution presented in Fig. 3(c). In order to identify a B^+ candidate sample, a least-squares fit similar to that imposed on the $J/\psi K_S^0$ candidates was performed. We required that the confidence level of this fit be greater than 0.01, and that the $c\tau$ of the K_S^0 candidate be greater than 0.1 cm. The transverse momentum of the B^+ candidate had to exceed 6.0 GeV/c and its $c\tau$ had to be positive. In order to isolate a $K^*(892)^+$ resonance, we required that the invariant $K_S^0 \pi^+$ mass be within $0.08 \text{ GeV}/c^2$ of the world average $K^*(892)^+$

TABLE I. The definition of the signal regions, sideband regions, and the number of observed events associated with the decays $B^+ \rightarrow J/\psi K^* \pi^+$, $B^0 \rightarrow J/\psi K^* \pi^0$, and $B_s^0 \rightarrow J/\psi \phi$. The number of observed events is calculated in three ways: fitting the resonant structure in the $K\pi$ and KK invariant mass distributions either using the sideband distributions to estimate the background (N_{sb}) or using a second-order polynomial to estimate the background (N_{fit}), and using the number of observed B candidate events, correcting for the loss of resonant decays due to the two-body mass requirement (N_{win}). The number of events obtained using the sideband subtracted background, N_{sb} , is used to calculate the branching fraction ratios.

	$J/\psi K_s^0 \pi^+$	$J/\psi K^+ \pi^-$	$J/\psi K^+ K^-$
Signal region (GeV/c^2)	5.235–5.325	5.235–5.325	5.320–5.410
Sideband regions (GeV/c^2)	5.000–5.220	5.000–5.180	5.100–5.305
	5.340–5.600	5.380–5.600	5.425–5.700
N_{sb} (events)	21.3 ± 6.1	119 ± 20	26.7 ± 7.3
N_{fit} (events)	17.0 ± 6.5	108 ± 27	27.3 ± 7.4
N_{win} (events)	16.0 ± 5.3	119 ± 18	34.4 ± 7.3

mass ($0.8916 \text{ GeV}/c^2$) [13]. This results in the $J/\psi K_s^0 \pi^+$ invariant mass distribution shown in Fig. 2(c). A fit of this distribution to a Gaussian line shape and linear background results in an estimated signal of 12.9 ± 4.3 decays.

4. The $B^0 \rightarrow J/\psi K^*(892)^0$ channel

Our data selection to reconstruct the decay $B^0 \rightarrow J/\psi K^*(892)^0 \rightarrow J/\psi K^+ \pi^-$ proceeded in a similar manner. We formed combinations of all oppositely charged track pairs, and fit the four charged tracks requiring that they come from a common decay point, constraining the invariant dimuon mass to the world average J/ψ mass, and requiring that the flight path of the B^0 candidate be parallel to its momentum vector in the transverse plane. The confidence level of this fit had to be greater than 0.01 and the B^0 candidate $c\tau$ had to be positive. The combinatorial backgrounds to the $K^*(892)^0$ decay are also large. This is illustrated in Fig. 3(d), where we show the $K^+ \pi^-$ invariant mass distribution for events that have transverse momentum of the $K^+ \pi^-$ system greater than $2.0 \text{ GeV}/c$. We defined the B^0 candidate sample by requiring the P_T of the $K^+ \pi^-$ system to be greater than $2.0 \text{ GeV}/c$ and the resulting $J/\psi K^+ \pi^-$ system to have $P_T > 8.0 \text{ GeV}/c$. We required the $K^+ \pi^-$ invariant mass to be within $0.08 \text{ GeV}/c^2$ of the world average $K^*(892)^0$ mass ($0.8961 \text{ GeV}/c^2$). The resulting $J/\psi K^+ \pi^-$ invariant mass distribution is shown in Fig. 2(d).

The peak in Fig. 2(d) also has contributions from $K^*(892)^0$ decays where the incorrect kaon and pion mass assignments yield an invariant $K^+ \pi^-$ mass within the $K^*(892)^0$ mass window of $\pm 0.08 \text{ GeV}/c^2$. We used a Monte Carlo calculation, described in Sec. IV, to determine the relative fraction of such combinations and the shape of the resulting $J/\psi K^+ \pi^-$ invariant mass distribution. The signal shape was parametrized by two Gaussian distributions with the relative width, normalization, and position of the second distribution determined by a fit to the $J/\psi K^+ \pi^-$ invariant mass distribution predicted by the Monte Carlo calculation. The width of the second Gaussian was fixed to 3.3 times the width of the first, the normalization of the second was fixed to 0.08 times that of the first, and the mean of the second Gaussian distribution was offset lower in mass by $0.0023 \text{ GeV}/c^2$ relative to the mean of the first. This shape then was used in a fit to the observed $J/\psi K^*(892)^0$ invariant mass

distribution to determine the number of B^0 decays in our data. This procedure yields a signal of 95.5 ± 14.3 $B^0 \rightarrow J/\psi K^*(892)^0$ decays.

5. The $B_s^0 \rightarrow J/\psi \phi(1020)$ channel

The search for the decay mode $B_s^0 \rightarrow J/\psi \phi(1020) \rightarrow J/\psi K^+ K^-$ was performed by considering as $\phi(1020) \rightarrow K^+ K^-$ candidates all oppositely charged track pairs. A least-squares fit of the $\mu^+ \mu^- K^+ K^-$ candidate system was performed, constraining all four tracks to come from the same vertex, constraining the dimuon invariant mass to the world average J/ψ mass, and imposing a two-dimensional pointing constraint on the B_s^0 decay. The confidence level of this fit had to exceed 0.01. A $\phi(1020)$ signal of $(4.1 \pm 0.4) \times 10^3$ events is evident in this sample, as illustrated in Fig. 3(b). The combinatorial background was reduced by requiring the $K^+ K^-$ system to have $P_T > 2.0 \text{ GeV}/c$, the $J/\psi K^+ K^-$ system to have $P_T > 6.0 \text{ GeV}/c$ and the $c\tau$ of the B_s^0 candidate system to be positive. We defined our $\phi(1020) \rightarrow K^+ K^-$ candidate sample by requiring the $K^+ K^-$ invariant mass to be within $0.0100 \text{ GeV}/c^2$ of the world average ϕ mass ($1.0194 \text{ GeV}/c^2$) [13]. This resulted in a sample with the $J/\psi K^+ K^-$ invariant mass distribution shown in Fig. 2(e). A B_s^0 signal is evident on a relatively small background. A fit of this distribution to a Gaussian line shape and linear background results in a total signal of 29.4 ± 6.2 events.

III. RESONANT AND NONRESONANT DECAYS

Clear signals for B meson production and decay are observed in all five channels. In the case of the three channels involving a $K^*(892)$ or $\phi(1020)$ resonance in the final state, the estimated number of B candidate events includes resonant and nonresonant contributions in the final state. We searched for evidence of a nonresonant $K\pi$ or KK contribution to the B meson signals by placing invariant mass cuts on the B candidate, removing the invariant mass cuts on the two-meson systems and examining the $K_s^0 \pi^-$, $K^+ \pi^-$, and $K^+ K^-$ invariant mass distributions. In order to account for non- B background in the two-body mass distributions, we defined B mass sideband regions for the three samples, normalized to the estimated number of non- B events as determined from the B invariant mass distributions. The signal

and sideband regions are described in Table I. By allowing for a nonresonant contribution to the B decay rate, we will estimate directly the rate of resonant decays without having to assume that the rate of nonresonant decays is negligible.

The $K_S^0\pi^+$, $K^+\pi^-$, and K^+K^- invariant mass distributions are illustrated in Fig. 4 for the B signal and sideband regions (the shaded distributions are from candidates in the B sideband regions normalized to the background under the B meson peak in the signal region). One sees from these distributions resonant signals for the $K^*(892)$ and $\phi(1020)$. We quantified the amount of resonance production associated with the B signals by performing binned maximum likelihood fits of the two-body invariant mass distributions to Breit-Wigner line shapes convoluted with detector resolution. We used the observed B sideband distributions to model the shape of the background under the two-body resonance signals. The resulting numbers of observed events, N_{sb} , are listed in Table I. As a cross-check, we also estimated the number of signal events by fitting the resonance signals to Breit-Wigner line shapes convoluted with detector resolution and background shapes described by second-order polynomial functions. The resulting event rates, N_{fit} , are listed in Table I and are consistent with N_{sb} .

Under the assumption that there are no nonresonant decays, we also can estimate the strength of the two-body resonant decay by correcting the observed B rates determined from the fits to the $J/\psi K\pi$ and $J/\psi KK$ invariant mass distributions in Fig. 2(c)–(e) for the loss in efficiency due to the $K\pi$ and KK mass cuts. The presence of nonresonant $K\pi$ or KK decays would result in corrected B decay rates systematically larger than those determined by N_{sb} or N_{fit} . The mass cut efficiencies have been estimated using a Monte Carlo calculation to be 0.80 and 0.86 for the $K\pi$ and KK mass window cuts, respectively. The resulting B meson rates, N_{win} , are listed in Table I. We see no significant difference in the rates estimated by these three methods. We, therefore, conclude that we do not observe a significant nonresonant $B \rightarrow J/\psi K\pi$ or $B_s^0 \rightarrow J/\psi KK$ decay mode.

For the subsequent analysis, we choose N_{sb} as the best estimate of the rate of resonant production as it is least biased by potential contributions from nonresonant production. In addition, we have investigated the possibility that kinematic reflections of other B hadron decay modes could enhance our observed event yields, and have excluded such contributions.

IV. EFFICIENCY CORRECTIONS

We estimate the relative reconstruction efficiency for each B meson decay mode to convert the observed number of B events into ratios of branching fractions. We write the efficiencies for reconstructing B mesons as

$$\epsilon^{K^+} = \epsilon_{J/\psi} \times \epsilon_{\text{geom}}^{K^+} \times \epsilon_{c\tau}^{K^+} \times \epsilon_K, \quad (7)$$

$$\epsilon^{K^0} = \epsilon_{J/\psi} \times \epsilon_{\text{geom}}^{K^0} \times \epsilon_{c\tau}^{K^0} \times \epsilon_{K_S}, \quad (8)$$

$$\epsilon^{K^{*+}} = \epsilon_{J/\psi} \times \epsilon_{\text{geom}}^{K^{*+}} \times \epsilon_{c\tau}^{K^{*+}} \times \epsilon_{K_S} \times \epsilon_\pi, \quad (9)$$

$$\epsilon^{K^{*0}} = \epsilon_{J/\psi} \times \epsilon_{\text{geom}}^{K^{*0}} \times \epsilon_{c\tau}^{K^{*0}} \times \epsilon_K \times \epsilon_\pi, \quad (10)$$

$$\epsilon^\phi = \epsilon_{J/\psi} \times \epsilon_{\text{geom}}^\phi \times \epsilon_{c\tau}^\phi \times \epsilon_\phi, \quad (11)$$

where we show the common contributions. The quantity $\epsilon_{J/\psi}$ is the efficiency for triggering and reconstructing the $J/\psi \rightarrow \mu^+\mu^-$ decay. It is common to all decay modes. This also includes the combined efficiencies of the vertex and vertex-plus-mass constrained fits of 0.952 ± 0.006 , which cancels out in our subsequent analysis. The quantities ϵ_{geom} are the geometrical efficiencies for finding the daughter mesons in the tracking fiducial volume, having the decay exceed the minimum P_T requirements on the meson and B systems given a J/ψ candidate, and having the B candidate satisfy the constrained fit requirements. The quantities $\epsilon_{c\tau}$ are the efficiencies of the proper decay length requirement on the B candidate in the different decay modes. The quantities ϵ_K , ϵ_{K_S} , ϵ_π , and ϵ_ϕ are the efficiencies for reconstructing the K^+ , K_S^0 , π^- , and ϕ mesons using the charged track information.

In addition to these efficiencies, we correct the observed event rates for the relevant branching fractions into intermediate states, $\mathcal{B}(K^0 \rightarrow K_S^0 \rightarrow \pi^+\pi^-) = 0.3430 \pm 0.0014$ and $\mathcal{B}(\phi(1020) \rightarrow K^+K^-) = 0.491 \pm 0.009$, both taken from Ref. [13], and the isospin weighting factors $\mathcal{B}(K^*(892)^0 \rightarrow K^+\pi^-) = \mathcal{B}(K^*(892)^+ \rightarrow K^0\pi^+) = 2/3$.

Since we are only interested in ratios of efficiencies, the common terms in these efficiencies cancel, reducing the overall uncertainties. These include the term $\epsilon_{J/\psi}$, and the reconstruction efficiencies ϵ_K or ϵ_{K_S} when they appear in both the numerator and denominator of the ratio. A number of other quantities do not cancel necessarily when calculating the ratio of branching fractions. In order to evaluate the relative efficiencies, we employed a B meson Monte Carlo calculation. B mesons were generated with a P_T spectrum predicted by a next-to-leading order QCD calculation [15] using the Martin-Roberts-Stirling set D0 (MRS D0) parton distribution functions [16]. The b quark P_T was required to be >5 GeV/ c , and the b quark fragmentation into a B meson was modeled using the Peterson parametrization with the parameter ϵ chosen to be 0.006 [17]. The B mesons were decayed using the CLEO B decay model [18] and a full simulation was used to model the response of the CDF detector, including effects due to the underlying event. The resulting Monte Carlo events were then processed with the same algorithms used to reconstruct the data. We used the reconstructed Monte Carlo events to estimate the geometrical acceptances ϵ_{geom} . These efficiencies are listed in Table II.

The geometrical efficiencies include the effect of the B meson vertex and mass constrained fits. We determined that the efficiency of the fitting procedure and subsequent confidence level requirements were independent of B decay mode by measuring the relative loss in signal events when different event topologies were fit employing both a vertex constraint and a vertex-plus-mass constraint. We assigned a systematic uncertainty of 1% in the relative acceptances to this effect, which we estimated by comparing the relative loss of signal events in the different decay topologies. We also investigated the uncertainties associated with the model of the detector used to measure the reconstruction efficiencies. We verified that the detector simulations described accurately the interaction vertex distributions and detector geometry. We then compared the efficiencies determined using the complete de-

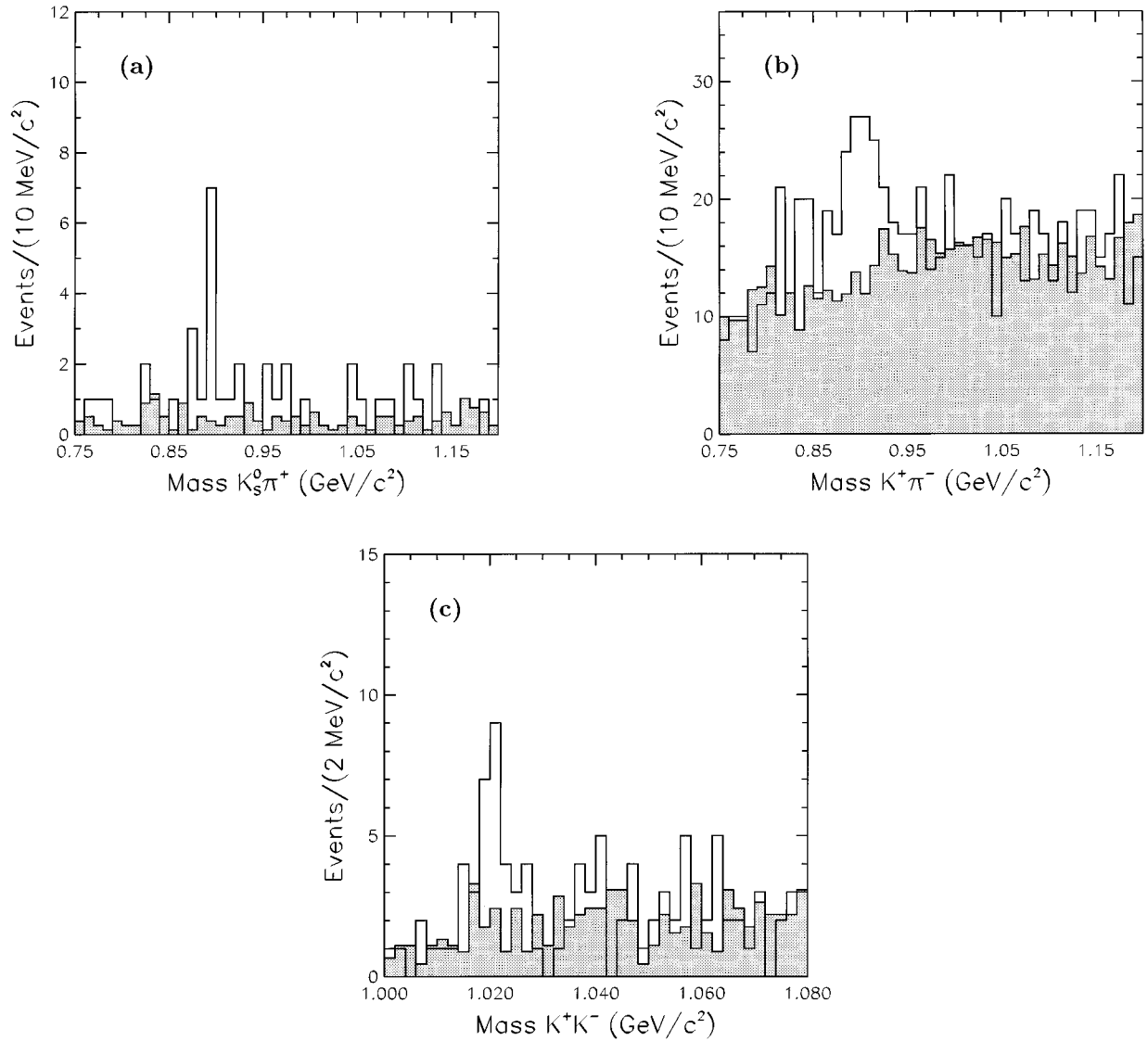


FIG. 4. The $K_S^0\pi^+$ invariant mass distributions for the B^+ signal and sideband regions are shown in (a). The B^+ signal region is represented by the unshaded histogram. The B^+ sideband region, normalized to the non- B^+ background in the B^+ signal region, is the shaded distribution. The corresponding distributions for the $K^+\pi^-$ and K^+K^- invariant mass are shown in (b) and (c), respectively.

tector simulation to those determined using a parametrized model of the detector. Based on this comparison, we assigned a 5% systematic uncertainty on the relative geometrical efficiencies to take into account any remaining uncertainties in the detector model.

In principle, the B meson $c\tau$ requirements have different efficiencies for each channel because of different momentum and vertex resolutions for the final states and possible differences in the lifetimes of the B meson states. We evaluated the efficiencies $\epsilon_{c\tau}$ using the world average values for the

TABLE II. The number of observed signal events and the reconstruction efficiencies for the five decay modes. The geometrical efficiency includes the meson P_T requirements and the acceptance of the tracking fiducial volume. It does not include the J/ψ and light quark meson branching fractions. The efficiencies of the B proper decay length requirement and the reconstruction efficiencies of the light quark mesons also are listed. Some of the systematic uncertainties are correlated as they have common sources. These correlations are taken into account when ratios of the observed decay rates are determined.

Channel	Events	ϵ_{geom}	$\epsilon_{c\tau}$	ϵ_{meson}
$B^+ \rightarrow J/\psi K^+$	154 ± 19	$(10.1 \pm 0.8) \times 10^{-2}$	0.900 ± 0.005	0.979 ± 0.031
$B^0 \rightarrow J/\psi K^0$	36.9 ± 7.3	$(7.95 \pm 0.58) \times 10^{-2}$	0.876 ± 0.007	0.857 ± 0.012
$B^+ \rightarrow J/\psi K^{*+}$	21.3 ± 6.1	$(4.17 \pm 0.30) \times 10^{-2}$	0.880 ± 0.006	0.839 ± 0.015
$B^0 \rightarrow J/\psi K^{*0}$	119 ± 20	$(8.39 \pm 0.59) \times 10^{-2}$	0.893 ± 0.006	0.958 ± 0.032
$B_s^0 \rightarrow J/\psi \phi$	26.7 ± 7.3	$(10.7 \pm 0.8) \times 10^{-2}$	0.884 ± 0.020	0.904 ± 0.058

lifetimes of the three B mesons [13], using tracking detector resolutions observed in the events in the B sideband regions. The results are listed in Table II. We repeated the efficiency calculation varying the lifetimes by one standard deviation. The resulting variations in the relative efficiencies were assigned as systematic uncertainties.

The meson reconstruction efficiencies take into account the charged track reconstruction efficiencies, the efficiencies of the K_S^0 lifetime cut and the additional constrained fits performed when a K_S^0 candidate is in the final state. The track reconstruction efficiencies were determined using both a full detector simulation and by embedding simulated tracks in real interactions containing J/ψ candidates. The systematic uncertainties in the track reconstruction efficiencies were determined by varying the embedding techniques. The loss of K^\pm mesons due to decays-in-flight was estimated using the full detector simulation. Between 4% and 6% of K^\pm mesons (depending on the B meson decay mode) decay within the volume of the CTC, of which approximately 40% are reconstructed correctly. We assigned a 3% systematic uncertainty on ϵ_K due to the decays-in-flight correction.

The K_S^0 lifetime cut efficiency and the efficiencies of the vertex and mass constrained fits were determined by measuring the loss of signal events in both the proper lifetime distribution and the $\pi^+\pi^-$ invariant mass distributions. The efficiency of the lifetime cut was determined to be 0.958 ± 0.007 . The uncertainty represents the difference in efficiencies determined by estimating the loss of real K_S^0 decays using the $\pi^+\pi^-$ invariant mass and the $c\tau$ distributions for the candidate samples. The fractions of K_S^0 candidates that satisfied the confidence level requirements on the vertex and vertex-plus-mass constrained fits were 0.938 ± 0.017 and 0.983 ± 0.006 , respectively.

A number of additional checks were made to verify that correlations in efficiencies were taken properly into account. The variation of the dimuon trigger acceptance for the different B meson final states was determined using a Monte Carlo calculation that simulated both the detector response and the effect of the trigger. This resulted in a negligible uncertainty in the ratio of acceptances. Variations in the P_T spectrum of the produced B mesons also could result in a change in the relative acceptance. This was measured by varying the renormalization scale and the b quark mass in the Monte Carlo calculation of this spectrum. We assigned a systematic uncertainty on the relative acceptance due to this effect that varies from 1% to 5%, depending on the pair of final states being compared. The polarization of the vector mesons in the final state also has an effect on the relative acceptance. We varied the longitudinal polarization of the $K^*(892)$ meson in the B meson rest frame by ± 0.10 around

TABLE III. The systematic uncertainties in the relative efficiencies for the different channels.

Effect	Systematic uncertainty (%)
B meson confidence level requirements	1
Detector simulation	5
K^+ reconstruction efficiency	1
Vector meson polarization	2.5
K_S^0 reconstruction	1
$B P_T$ spectrum	1–5
Effects of excited B meson production	1–4

a nominal value of 0.75 and the $\phi(1020)$ meson longitudinal polarization by ± 0.25 around the nominal value of 0.50 [19]. We assigned the resulting 2.5% change in acceptance as the systematic uncertainty due to this effect.

We expect B^+ , B^0 , and B_s^0 mesons to be produced both directly and through the production of excited B meson states that decay to the pseudoscalar mesons we observe. We investigated the effect such resonant production would have on the relative ratio of efficiencies of the decay modes studied by performing a Monte Carlo calculation using the PYTHIA program [20], which models the production and decay of higher mass B meson states. In this calculation, we assumed that the relative production of B mesons with orbital angular momentum L and spin S was in the ratio 0.30:0.53:0.17 for $L=1$ and $S=0$ or 1: $L=0$ and $S=1$: $L=0$ and $S=0$ [21]. The change in the ratio of acceptances, relative to the case where only pseudoscalar meson production was assumed, varied from 1% to 4%, depending on the decay mode considered. We included this as an additional systematic uncertainty on the acceptance.

The systematic uncertainties assigned to the relative efficiencies are summarized in Table III. These were combined in quadrature to determine the total systematic uncertainty on the relative acceptance for each pair of decay modes used in this study.

V. RESULTS

We present our results as a matrix of ratios of acceptance-corrected rates of B meson decays into the five channels. The observed numbers of signal events, listed in Table II, were corrected by the detection efficiency for each decay. When we form the ten possible ratios of these acceptance-corrected event rates, the b quark production cross section and the common efficiencies cancel. The results are listed in Table IV. Three of these ratios also have been determined using a

TABLE IV. The ratios of fragmentation fractions times branching fractions for the various B meson final states. The ratio R_i^j is located in the i th row and j th column. The uncertainties are statistical and systematic, respectively.

	$(J/\psi K^0)$	$(J/\psi K^{*+})$	$(J/\psi K^{*0})$	$(J/\psi \phi)$
$(J/\psi K^+)$	$1.15 \pm 0.27 \pm 0.09$	$1.92 \pm 0.60 \pm 0.17$	$1.59 \pm 0.33 \pm 0.12$	$0.41 \pm 0.12 \pm 0.04$
$(J/\psi K^0)$		$1.68 \pm 0.58 \pm 0.11$	$1.39 \pm 0.36 \pm 0.10$	$0.35 \pm 0.12 \pm 0.03$
$(J/\psi K^{*+})$			$0.83 \pm 0.27 \pm 0.07$	$0.21 \pm 0.08 \pm 0.02$
$(J/\psi K^{*0})$				$0.26 \pm 0.08 \pm 0.02$

different technique based on the same data set [10]. The values determined here are in good agreement with these previous results. Note that the two measurements of these three ratios are not statistically independent.

The measured quantities are the ratios of the product of b quark fragmentation fractions and the B meson branching fractions into the specific final state. Thus our measurements can be written as

$$R_{K^+}^{K^0} = \frac{f_d}{f_u} \frac{\mathcal{B}(B^0 \rightarrow J/\psi K^0)}{\mathcal{B}(B^+ \rightarrow J/\psi K^+)} = 1.15 \pm 0.27 \pm 0.09, \quad (12)$$

$$R_{K^+}^{K^{*+}} = \frac{\mathcal{B}(B^+ \rightarrow J/\psi K^{*+})}{\mathcal{B}(B^+ \rightarrow J/\psi K^+)} = 1.92 \pm 0.60 \pm 0.17, \quad (13)$$

$$R_{K^+}^{K^{*0}} = \frac{f_d}{f_u} \frac{\mathcal{B}(B^0 \rightarrow J/\psi K^{*0})}{\mathcal{B}(B^+ \rightarrow J/\psi K^+)} = 1.59 \pm 0.33 \pm 0.12, \quad (14)$$

$$R_{K^+}^{K^\phi} = \frac{f_s}{f_u} \frac{\mathcal{B}(B_s^0 \rightarrow J/\psi \phi)}{\mathcal{B}(B^+ \rightarrow J/\psi K^+)} = 0.41 \pm 0.12 \pm 0.04, \quad (15)$$

$$R_{K^0}^{K^{*+}} = \frac{f_u}{f_d} \frac{\mathcal{B}(B^+ \rightarrow J/\psi K^{*+})}{\mathcal{B}(B^0 \rightarrow J/\psi K^0)} = 1.68 \pm 0.58 \pm 0.11, \quad (16)$$

$$R_{K^0}^{K^{*0}} = \frac{\mathcal{B}(B^0 \rightarrow J/\psi K^{*0})}{\mathcal{B}(B^0 \rightarrow J/\psi K^0)} = 1.39 \pm 0.36 \pm 0.10, \quad (17)$$

$$R_{K^0}^{K^\phi} = \frac{f_s}{f_d} \frac{\mathcal{B}(B_s^0 \rightarrow J/\psi \phi)}{\mathcal{B}(B^0 \rightarrow J/\psi K^0)} = 0.35 \pm 0.12 \pm 0.03, \quad (18)$$

$$R_{K^{*+}}^{K^{*0}} = \frac{f_d}{f_u} \frac{\mathcal{B}(B^0 \rightarrow J/\psi K^{*0})}{\mathcal{B}(B^+ \rightarrow J/\psi K^{*+})} = 0.83 \pm 0.27 \pm 0.07, \quad (19)$$

$$R_{K^{*+}}^{K^\phi} = \frac{f_s}{f_u} \frac{\mathcal{B}(B_s^0 \rightarrow J/\psi \phi)}{\mathcal{B}(B^+ \rightarrow J/\psi K^{*+})} = 0.21 \pm 0.08 \pm 0.02, \quad (20)$$

$$R_{K^{*0}}^{K^\phi} = \frac{f_s}{f_d} \frac{\mathcal{B}(B_s^0 \rightarrow J/\psi \phi)}{\mathcal{B}(B^0 \rightarrow J/\psi K^{*0})} = 0.26 \pm 0.08 \pm 0.02, \quad (21)$$

where the first and second uncertainties are the statistical and systematic uncertainties, respectively (henceforth the first and second uncertainties in measured values will represent the statistical and systematic uncertainties, respectively).

We can use these data to constrain both the fragmentation fractions and the meson branching fractions. To extract the branching fractions, we will have to assume certain ratios of fragmentation fractions. Correspondingly, we will use phenomenological and theoretical predictions for the ratios of branching fractions to extract the fragmentation fractions.

A. Branching fractions

1. The B_s^0 branching fraction

The ratios of branching fractions that involve the B_s^0 meson can be used with the world average values for the B^+ and B^0 meson branching fractions into the four other final states [13] to estimate the product of the ratio of fragmentation fractions, $f_s/(f_u, f_d)$, times the branching fraction $\mathcal{B}(B_s^0 \rightarrow J/\psi \phi)$. The world average B^+ and B^0 branching frac-

tions have been measured assuming that the fragmentation fractions f_u and f_d are equal for b quarks produced in $Y(4S)$ decays, and so this assumption is implicit in this calculation.

All ratios that involve the B_s^0 can be rewritten in the form given by the example

$$f_s \mathcal{B}(B_s^0 \rightarrow J/\psi \phi) = f_u \mathcal{B}(B^+ \rightarrow J/\psi K^+) R_{K^+}^\phi, \quad (22)$$

which gives us four different measures of the ratio of fragmentation fractions and the B_s^0 branching fraction, using the world average values for the branching fractions [13] on the right-hand side of Eq. (22). With the assumption of equal B^+ and B^0 fragmentation fractions, we form the weighted average of the four estimates to obtain

$$\frac{f_s}{(f_u, f_d)} \mathcal{B}(B_s^0 \rightarrow J/\psi \phi) = (0.37 \pm 0.11 \pm 0.04) \times 10^{-3}. \quad (23)$$

In order to extract $\mathcal{B}(B_s^0 \rightarrow J/\psi \phi)$, we assume $f_u = f_d$ and use the value $f_s = (0.40 \pm 0.06)f_u$. This value of f_s represents the central value of the range of reported f_s measurements [11,12], and the uncertainty has been chosen to cover half of the difference between the minimum and maximum values. It is also consistent with the suppression of strange hadrons observed in the production of light quark hadrons [24]. With these values for the fragmentation fractions, we determine

$$\mathcal{B}(B_s^0 \rightarrow J/\psi \phi) = (0.93 \pm 0.28 \pm 0.10 \pm 0.14) \times 10^{-3}. \quad (24)$$

The first uncertainty is statistical, the second accounts for the systematic uncertainties associated with the ratio of branching fraction measurements, and the third is the uncertainty associated with the value we have taken for f_s .

2. The B^+ and B^0 branching fractions

We also can use these data to estimate the branching fractions $\mathcal{B}(B^+ \rightarrow J/\psi K^+)$, $\mathcal{B}(B^0 \rightarrow J/\psi K^0)$, $\mathcal{B}(B^+ \rightarrow J/\psi K^{*+})$, and $\mathcal{B}(B^0 \rightarrow J/\psi K^{*0})$ using the world average values for the branching fractions, our ratios of branching fractions, and the assumption that $f_u = f_d$. For example, for the decay $B^+ \rightarrow J/\psi K^{*+}$, we have three separate estimates

$$\mathcal{B}(B^+ \rightarrow J/\psi K^{*+}) = \mathcal{B}(B^+ \rightarrow J/\psi K^+) R_{K^+}^{K^{*+}}, \quad (25)$$

$$\mathcal{B}(B^+ \rightarrow J/\psi K^{*+}) = \mathcal{B}(B^0 \rightarrow J/\psi K^0) \left(\frac{f_d}{f_u} \right) R_{K^0}^{K^{*+}}, \quad (26)$$

$$\mathcal{B}(B^+ \rightarrow J/\psi K^{*+}) = \mathcal{B}(B^0 \rightarrow J/\psi K^{*0}) \left(\frac{f_d}{f_u} \right) \frac{1}{R_{K^{*+}}^{K^{*0}}}. \quad (27)$$

We use for the first factor on the right-hand side of these estimates the world average values for the branching fractions [13] and form the weighted average of these three measurements, thereby reducing the net statistical uncertainty. Because we employ in this calculation the world averages that have been determined assuming that $f_u = f_d$, these results depend implicitly on this assumption. Note that this estimate of $\mathcal{B}(B^+ \rightarrow J/\psi K^{*+})$ is statistically independent of the world average value for this branching fraction.

Using this procedure, we obtain the branching fractions

$$\mathcal{B}(B^+ \rightarrow J/\psi K^+) = (0.82 \pm 0.18 \pm 0.07) \times 10^{-3}, \quad (28)$$

$$\mathcal{B}(B^0 \rightarrow J/\psi K^0) = (1.14 \pm 0.27 \pm 0.09) \times 10^{-3}, \quad (29)$$

$$\mathcal{B}(B^+ \rightarrow J/\psi K^{*+}) = (1.73 \pm 0.55 \pm 0.15) \times 10^{-3}, \quad (30)$$

$$\mathcal{B}(B^0 \rightarrow J/\psi K^{*0}) = (1.39 \pm 0.32 \pm 0.11) \times 10^{-3}. \quad (31)$$

The statistical and systematic uncertainties have been estimated by weighting the relative contributions in the world average values and our data. The uncertainties in the world average branching fractions used in this calculation are dominated by the most recent measurements by the CLEO Collaboration [5]. These uncertainties are limited by the size of the CLEO sample, and are, therefore, largely statistical and independent. We have examined the stability of these estimates to different assumptions concerning the independence of the quoted systematic uncertainties. We find that our results and their estimated uncertainties are insensitive to possible correlations in the systematic uncertainties in the CLEO measurements.

3. Comparison with theory

We have compared our measured ratios of branching fractions times fragmentation fractions with a calculation of the two-body nonleptonic decay rates of B mesons, using the factorization hypothesis, chiral and heavy quark symmetries, and data from semileptonic D meson decays [3]. We adjusted the predicted ratios by the world average B meson lifetimes [13] to correct for the observed lifetime differences of these three states. Although several recent theoretical calculations of these branching fractions exist, we have selected Ref. [3] for this comparison as it predicts all the branching fractions for the five decays studied here. The other model calculations have been made with varying theoretical assumptions and observational constraints, but they generally predict ratios of branching fractions that are in reasonable agreement with each other and our observations. It should be noted that these calculations generally assume the validity of factorization as applied to nonleptonic B meson decays, but they differ in many details, such as the magnitude and shape of the form factors for B meson decay and the experimental constraints employed in the calculations. In Ref. [3], the form factors are normalized to D meson semileptonic decay data and are assumed to be consistent with simple pole dominance. This assumption has been criticized recently [22,23] in the light of data on the observed polarization in the decay $B \rightarrow J/\psi K^*$.

The results of the comparisons are shown in Fig. 5. In order to compare ratios involving B_s^0 decays, we have assumed $f_u = f_d$ and taken $f_s = (0.40 \pm 0.06)f_u$. The predictions agree well with the observed ratios of branching fractions for all the decay modes.

B. Ratios of meson fragmentation fractions

The b quark fragmentation fractions have not been measured directly in a hadron collider environment. Our data allow us to constrain the ratios of these fractions. However, we note that the measured branching fractions of the B^+ and B^0 mesons have been determined assuming equal fragmen-

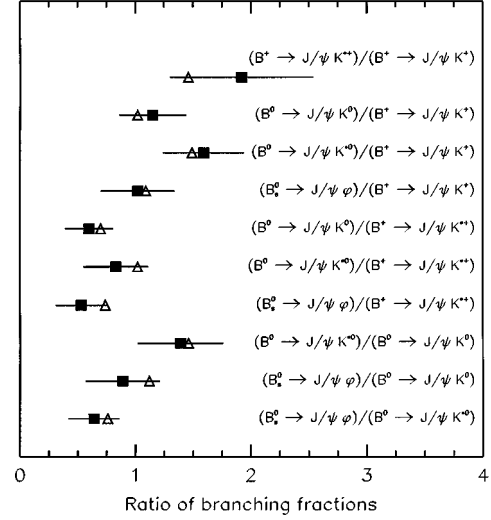


FIG. 5. Comparison of observed ratios of branching fractions (squares) with the theoretical prediction (triangles) described in the text. The error bars reflect the statistical and systematic uncertainties of the observed ratios added in quadrature.

tation fractions of b quarks produced in $Y(4S)$ decays. We, therefore, cannot employ the world average values for these quantities in estimating f_u , f_d , or f_s . Instead, we will make specific assumptions concerning the branching fractions.

Expressed in terms of fragmentation and branching fractions, the two ratios $R_{K^+}^{K^0}$ and $R_{K^{*+}}^{K^{*0}}$ give the relations

$$\frac{f_d}{f_u} = R_{K^+}^{K^0} \frac{\mathcal{B}(B^+ \rightarrow J/\psi K^+)}{\mathcal{B}(B^0 \rightarrow J/\psi K^0)}, \quad (32)$$

$$\frac{f_d}{f_u} = R_{K^{*+}}^{K^{*0}} \frac{\mathcal{B}(B^+ \rightarrow J/\psi K^{*+})}{\mathcal{B}(B^0 \rightarrow J/\psi K^{*0})}. \quad (33)$$

Under the assumption that the ratios of branching fractions on the right-hand side of Eqs. (32) and (33) are unity (which is the result of most quark model predictions), the weighted average of these two quantities gives

$$\frac{f_d}{f_u} = 0.99 \pm 0.19 \pm 0.08. \quad (34)$$

This result is consistent with the hypothesis that b quarks hadronize equally often into B^+ and B^0 mesons.

The strange meson fragmentation fraction f_s is constrained by the ratios that involve the B_s^0 final state, yielding the relationships

$$\frac{f_s}{f_u} = R_{K^{*+}}^\phi \frac{\mathcal{B}(B^+ \rightarrow J/\psi K^{*+})}{\mathcal{B}(B_s^0 \rightarrow J/\psi \phi)}, \quad (35)$$

$$\frac{f_s}{f_d} = R_{K^{*0}}^\phi \frac{\mathcal{B}(B^0 \rightarrow J/\psi K^{*0})}{\mathcal{B}(B_s^0 \rightarrow J/\psi \phi)}, \quad (36)$$

$$\frac{f_s}{f_u} = R_{K^+}^\phi \frac{\mathcal{B}(B^+ \rightarrow J/\psi K^+)}{\mathcal{B}(B_s^0 \rightarrow J/\psi \phi)}, \quad (37)$$

$$\frac{f_s}{f_d} = R_{K^0}^\phi \frac{\mathcal{B}(B^0 \rightarrow J/\psi K^0)}{\mathcal{B}(B_s^0 \rightarrow J/\psi \phi)}. \quad (38)$$

If we assume equal B^+ and B^0 decay rates to the $J/\psi K^*$ final states, equal B^+ and B^0 decay rates to the $J/\psi K$ final states and $f_u = f_d$, we obtain the ratios

$$\frac{f_s}{(f_u, f_d)} = (0.24 \pm 0.07 \pm 0.02) \frac{\mathcal{B}(B \rightarrow J/\psi K^*)}{\mathcal{B}(B_s^0 \rightarrow J/\psi \phi)}, \quad (39)$$

$$\frac{f_s}{(f_u, f_d)} = (0.39 \pm 0.11 \pm 0.04) \frac{\mathcal{B}(B \rightarrow J/\psi K)}{\mathcal{B}(B_s^0 \rightarrow J/\psi \phi)}. \quad (40)$$

The probability of B_s^0 meson production inferred from these data depends on the ratios of branching fractions in Eqs. (39) and (40). We take for the ratios of these fractions the values predicted in [3] and correct for lifetime differences as discussed earlier. We find that

$$\frac{f_s}{(f_u, f_d)} = 0.34 \pm 0.10 \pm 0.03. \quad (41)$$

In phenomenological fragmentation models, the probabilities f_u , f_d , and f_s are related to the relative probabilities of producing a $u\bar{u}$, $d\bar{d}$, and $s\bar{s}$ quark pair in the quark fragmentation process [25]. Measurements of the relative probabilities of strange meson to light meson production in e^+e^- and hadron-hadron collisions [11] and in deep inelastic scattering have yielded values in the range of 0.3 to 0.4. A recent compilation of these data has yielded a value of 0.29 ± 0.015 for the relative rate of strange quark production to up or down quark production [24], which agrees well with our values measured in b quark fragmentation. Taken together, these measurements indicate that the rate of $s\bar{s}$ suppression in quark fragmentation is largely independent of energy and flavor of the quark initiating the fragmentation process.

C. Fragmentation fractions of B hadrons

The hadronization of b quarks produces both B mesons and baryons. Most B hadron decay models predict that virtually all b baryons produced during the fragmentation process will decay subsequently via modes that include a Λ_b^0 baryon, and so we make that assumption here. A measurement of the rate of Λ_b^0 production in b quark fragmentation gives us a direct measure of f_{Λ_b} , the probability that a bottom quark will hadronize such that a Λ_b^0 baryon is produced. This, combined with our measurements of the ratios of fragmentation fractions, allows us to make a determination of the values of f_u , f_d , and f_s .

Studies of Λ_c^+ production in semileptonic b quark decays [26–28] have yielded measurements of the product

$$f_{\Lambda_b} \mathcal{B}(\Lambda_b^0 \rightarrow \Lambda_c^+ l^- \bar{\nu}_l X). \quad (42)$$

The naive spectator quark model would predict that the inclusive Λ_b^0 semileptonic branching fraction to a final state with a charm hadron X_c is in the range of 0.10. Reference [29] suggests a possible range of 0.10–0.13. We, therefore, have chosen to use the inclusive branching fraction $\mathcal{B}(\Lambda_b^0 \rightarrow X_c l^- \bar{\nu}_l) = 0.115$, the central value of the theoretical

prediction, to estimate f_{Λ_b} . Assuming this value and the three most recent measurements of Λ_b^0 production in b quark fragmentation, we find that $f_{\Lambda_b} = 0.096 \pm 0.017$. It is of interest to note that the observed ratio of meson to baryon production [24] in minimum bias $p\bar{p}$ collisions at $\sqrt{s} = 630$ GeV, 6.4 ± 1.1 , yields a baryon production fraction of 0.14 ± 0.02 . This is consistent with the value determined from Λ_b^0 semileptonic decays even though these two fractions are not necessarily expected to be equal.

Using the condition that the fragmentation fractions should sum to unity, assuming that the fraction of charm B hadrons $f_c \ll 1$ and all b baryons decay via Λ_b^0 intermediate states, then

$$f_u + f_d + f_s + f_{\Lambda_b} = 1. \quad (43)$$

This can be rearranged to determine values for f_u , f_d , and f_s using f_{Λ_b} and our measured ratios of fragmentation fractions:

$$f_u = \frac{1 - f_{\Lambda_b}}{1 + f_d/f_u + f_s/f_u}, \quad (44)$$

$$f_d = \frac{1 - f_{\Lambda_b}}{1 + f_u/f_d + f_s/f_d}, \quad (45)$$

$$f_s = \frac{1 - f_{\Lambda_b}}{1 + f_d/f_s + f_u/f_s}. \quad (46)$$

We find that $f_u = 0.39 \pm 0.04 \pm 0.04$, $f_d = 0.38 \pm 0.04 \pm 0.04$, and $f_s = 0.13 \pm 0.03 \pm 0.01$. These values are all proportional to the term $(1 - f_{\Lambda_b})$ and are, therefore, relatively insensitive to our assumption concerning the Λ_b^0 semileptonic branching fraction and our assumption that all b baryons decay to Λ_b^0 intermediate states.

VI. CONCLUSION

We have measured the ratios of branching fractions times fragmentation fractions for the five decay modes $B^+ \rightarrow J/\psi K^+$, $B^+ \rightarrow J/\psi K^*(892)^+$, $B^0 \rightarrow J/\psi K^0$, $B^0 \rightarrow J/\psi K^*(892)^0$, and $B_s^0 \rightarrow J/\psi \phi(1020)$.

We have used these measurements, with the assumption that $f_u = f_d$ and with $f_s = (0.40 \pm 0.06)f_u$, to determine the relative branching fractions of the B mesons into the observed final states. We have made the first measurement of a B_s^0 branching fraction to a final state with a J/ψ meson, yielding

$$\mathcal{B}(B_s^0 \rightarrow J/\psi \phi) = (0.93 \pm 0.28 \pm 0.10 \pm 0.14) \times 10^{-3}.$$

We also have used our data in conjunction with the current world average branching fractions to find

$$\mathcal{B}(B^+ \rightarrow J/\psi K^+) = (0.82 \pm 0.18 \pm 0.07) \times 10^{-3},$$

$$\mathcal{B}(B^0 \rightarrow J/\psi K^0) = (1.14 \pm 0.27 \pm 0.09) \times 10^{-3},$$

$$\mathcal{B}(B^+ \rightarrow J/\psi K^{*+}) = (1.73 \pm 0.55 \pm 0.15) \times 10^{-3},$$

$$\mathcal{B}(B^0 \rightarrow J/\psi K^{*0}) = (1.39 \pm 0.32 \pm 0.11) \times 10^{-3}.$$

These data are consistent with a B_s^0 branching fraction approximately equal to those of the B^+ and B^0 decays into topologically similar final states. The observed branching fractions are in good agreement with model calculations employing factorization, chiral symmetry, and heavy quark symmetries.

An analysis of the ratios of branching fractions supports the widely held assumption that the probabilities of producing B^+ and B^0 mesons in b quark fragmentation are equal. We measured the ratio of f_d to f_u to be $0.99 \pm 0.19 \pm 0.08$. If we assume the theoretically predicted ratios of branching fractions for the $B_s^0 \rightarrow J/\psi \phi(1020)$ relative to topologically similar decay modes for the B^+ and B^0 mesons and we assume $f_u = f_d$, we determine that $f_s/f_u = 0.34 \pm 0.10 \pm 0.03$. Employing an estimate for the fraction of Λ_b^0 production in b quark fragmentation, $f_{\Lambda_b} = 0.096 \pm 0.017$, we determine $f_u = 0.39 \pm 0.04 \pm 0.04$, $f_d = 0.38 \pm 0.04 \pm 0.04$, and $f_s = 0.13 \pm 0.03 \pm 0.01$. Thus, our results imply a suppression of $s\bar{s}$

production relative to $u\bar{u}$ and $d\bar{d}$ production in b quark fragmentation similar to that measured in e^+e^- and deep inelastic scattering experiments.

Note added in proof. Subsequent to submission of this article, measurements of these fractions have been reported in [30].

ACKNOWLEDGMENTS

We thank the Fermilab staff and the technical staff at the participating institutions for their essential contributions to this research. This work was supported by the U.S. Department of Energy and the National Science Foundation, the Natural Sciences and Engineering Research Council of Canada, the Istituto Nazionale di Fisica Nucleare of Italy, the Ministry of Education, Science and Culture of Japan, the National Science Council of the Republic of China, and the A. P. Sloan Foundation.

-
- [1] S. L. Glashow, Nucl. Phys. **22**, 579 (1961); S. Weinberg, Phys. Rev. Lett. **19**, 1264 (1967); A. Salam, in *Elementary Particle Theory: Relativistic Groups and Analyticity (Nobel Symposium No. 8)*, edited by N. Svartholm (Almqvist and Wiksells, Stockholm, 1968), p. 367.
- [2] M. Wirbel, B. Stech, and M. Bauer, Z. Phys. C **29**, 637 (1985); **34**, 103 (1987).
- [3] A. Deandrea, N. Di Bartolomeo, R. Gatto, and G. Nardulli, Phys. Lett. B **318**, 549 (1993).
- [4] G. Kramer and W. F. Palmer, Phys. Rev. D **46**, 2969 (1992); **46**, 3197 (1992).
- [5] CLEO Collaboration, M. S. Alam *et al.*, Phys. Rev. D **50**, 43 (1994).
- [6] ARGUS Collaboration, H. Albrecht *et al.*, Z. Phys. C **48**, 543 (1990).
- [7] CDF Collaboration, F. Abe *et al.*, Phys. Rev. D **53**, 1051 (1996).
- [8] D0 Collaboration, S. Abachi *et al.*, Phys. Rev. Lett. **74**, 3548 (1995).
- [9] CDF Collaboration, F. Abe *et al.*, Phys. Rev. Lett. **75**, 1451 (1995).
- [10] CDF Collaboration, F. Abe *et al.*, Phys. Rev. Lett. **76**, 2015 (1996).
- [11] V. Ammosov *et al.*, Phys. Lett. **93B**, 210 (1980); TASSO Collaboration, R. Brandelik *et al.*, *ibid.* **117B**, 135 (1982); P. K. Malhotra and R. Orava, Z. Phys. C **17**, 85 (1983); JADE Collaboration, W. Bartel *et al.*, Z. Phys. C **20**, 187 (1983); H. Aihara *et al.*, Phys. Rev. Lett. **53**, 2378 (1984); UA5 Collaboration, G. J. Alner *et al.*, Nucl. Phys. **B258**, 505 (1985); UA5 Collaboration, R. E. Ansorge *et al.*, Z. Phys. C **41**, 179 (1988); D. Bortoletto *et al.*, Phys. Rev. D **37**, 1719 (1988); F. Abe *et al.*, *ibid.* **40**, 3791 (1989).
- [12] DELPHI Collaboration, P. Abreu *et al.*, Z. Phys. C **61**, 407 (1994).
- [13] Particle Data Group, L. Montanet *et al.*, Phys. Rev. D **50**, 1173 (1994).
- [14] F. Abe *et al.*, Nucl. Instrum. Methods Phys. Res. A **271**, 387 (1988); D. Amidei *et al.*, *ibid.* **350**, 73 (1994); CDF Collaboration, F. Abe *et al.*, Phys. Rev. D **52**, 4784 (1995).
- [15] P. Nason, S. Dawson, and R. K. Ellis, Nucl. Phys. **B327**, 49 (1989); M. L. Mangano, P. Nason, and G. Ridolfi, *ibid.* **B373**, 295 (1992).
- [16] A. D. Martin, W. J. Stirling, and R. G. Roberts, Phys. Rev. D **47**, 867 (1993).
- [17] C. Peterson, D. Schlatter, I. Schmitt, and P. M. Zerwas, Phys. Rev. D **27**, 105 (1983); J. Chrin, Z. Phys. C **36**, 163 (1987).
- [18] P. Avery, K. Read, and G. Trahern, Cornell Internal Note CSN-212, 1985 (unpublished).
- [19] CDF Collaboration, F. Abe *et al.*, Phys. Rev. Lett. **75**, 3068 (1995).
- [20] T. Sjöstrand, Comput. Phys. Commun. **82**, 74 (1994). PYTHIA Version 5.7 was used.
- [21] DELPHI Collaboration, P. Abreu *et al.*, Z. Phys. C **68**, 353 (1995); L3 Collaboration, M. Acciarri *et al.*, Phys. Lett. B **345**, 589 (1995); ALEPH Collaboration, D. Buskulic *et al.*, Z. Phys. C **69**, 393 (1996).
- [22] M. Gourdin, A. N. Kamal, and X. Y. Pham, Phys. Rev. Lett. **73**, 3355 (1994).
- [23] R. Aleksan, A. Le Yaouanc, L. Oliver, O. Pène, and J.-C. Raynal, Phys. Rev. D **51**, 6235 (1995).
- [24] G. Bocquet *et al.*, Phys. Lett. B **366**, 447 (1996).
- [25] V. V. Anisovich and V. M. Shekhter, Nucl. Phys. **B55**, 455 (1973); R. D. Field and R. P. Feynman, *ibid.* **B136**, 1 (1978); B. Andersson, G. Gustafson, and B. Söderberg, Z. Phys. C **20**, 317 (1983).
- [26] DELPHI Collaboration, P. Abreu *et al.*, Z. Phys. C **68**, 375 (1995).
- [27] ALEPH Collaboration, D. Buskulic *et al.*, Phys. Lett. B **357**, 685 (1995).
- [28] OPAL Collaboration, R. Akers *et al.*, Z. Phys. C **69**, 195 (1996).
- [29] T. Mannel and G. A. Schuler, Phys. Lett. B **279**, 194 (1992).
- [30] Particle Data Group, R. M. Barnett *et al.*, Phys. Rev. D **54**, 1 (1996).